NeuroImage 220 (2020) 117095

Contents lists available at ScienceDirect

NeuroImage

journal homepage: www.elsevier.com/locate/neuroimage

Technical Note

Oxygen extraction fraction mapping with multi-parametric quantitative BOLD MRI: Reduced transverse relaxation bias using 3D-GraSE imaging

Stephan Kaczmarz [a,b,c,*], Fahmeed Hyder [b], Christine Preibisch [a,c,d]

[a] Technical University of Munich, School of Medicine, Klinikum rechts der Isar, Department of Diagnostic and Interventional Neuroradiology, Munich, Germany
[b] Departments of Radiology & Biomedical Imaging and of Biomedical Engineering, Magnetic Resonance Research Center, Yale University, New Haven, CT, 06520, USA
[c] Technical University of Munich, School of Medicine, Klinikum rechts der Isar, TUM Neuroimaging Center, Munich, Germany
[d] Technical University of Munich, School of Medicine, Klinikum rechts der Isar, Clinic for Neurology, Munich, Germany

ARTICLE INFO

Keywords:
Oxygen extraction fraction OEF
Multi-parametric quantitative BOLD
mq-BOLD
T_2
R_2'
3D GraSE

ABSTRACT

Magnetic resonance imaging (MRI)-based quantification of the blood-oxygenation-level-dependent (BOLD) effect allows oxygen extraction fraction (OEF) mapping. The multi-parametric quantitative BOLD (mq-BOLD) technique facilitates relative OEF (rOEF) measurements with whole brain coverage in clinically applicable scan times. Mq-BOLD requires three separate scans of cerebral blood volume and transverse relaxation rates measured by gradient-echo ($1/T_2$*) and spin-echo ($1/T_2$). Although the current method is of clinical merit in patients with stroke, glioma and internal carotid artery stenosis (ICAS), there are relaxation measurement artefacts that impede the sensitivity of mq-BOLD and artificially elevate reported rOEF values.

We posited that T_2-related biases caused by slice refocusing imperfections during rapid 2D-GraSE (**Gr**adient **a**nd **S**pin **E**cho) imaging can be reduced by applying 3D-GraSE imaging sequences, because the latter requires no slice selective pulses. The removal of T_2-related biases would decrease overestimated rOEF values measured by mq-BOLD. We characterized effects of T_2-related bias in mq-BOLD by comparing the initially employed 2D-GraSE and two proposed 3D-GraSE sequences to multiple single spin-echo reference measurements, both in vitro and in vivo. A phantom and 25 participants, including young and elderly healthy controls as well as ICAS-patients, were scanned. We additionally proposed a procedure to reliably identify and exclude artefact affected voxels. In the phantom, 3D-GraSE derived T_2 values had 57% lower deviation from the reference. For in vivo scans, the formerly overestimated rOEF was reduced by −27% ($p < 0.001$). We obtained rOEF = 0.51, which is much closer to literature values from positron emission tomography (PET) measurements. Furthermore, increased sensitivity to a focal rOEF elevation in an ICAS-patient was demonstrated.

In summary, the application of 3D-GraSE improves the mq-BOLD-based rOEF quantification while maintaining clinically feasible scan times. Thus, mq-BOLD with non-slice selective T_2 imaging is highly promising to improve clinical diagnostics of cerebrovascular diseases such as ICAS.

1. Introduction

As the brain has high energy demands without oxygen storage capacities, cerebral oxygen supply is crucial (Hyder, 2009). An important parameter of oxygen supply is the oxygen extraction fraction (OEF), which is defined as the ratio of oxygen consumed by the brain to oxygen delivered. OEF has high potential to improve diagnosis of cerebrovascular diseases (CVD) as a biomarker of hemodynamic function (Donahue et al., 2018). In patients with internal carotid artery stenosis (ICAS), correlations between higher OEF and increased stroke risks were found (Baron et al., 1981; Derdeyn et al., 2002; Powers et al., 2011) as well as local flow-metabolism uncoupling (Goettler et al., 2019). Furthermore, OEF is of interest for neuroscientific applications (Epp et al., 2019), as cerebral oxygen consumption supports neuronal activity (Hyder et al., 2002; Shu et al., 2016a, 2016b; Smith et al., 2002).

OEF measurements were originally established by ^{15}O labeled water PET (Donahue et al., 2018). However, its application is limited due to the administration of short-lived radioactive ^{15}O-tracers, invasive arterial blood sampling and restricted availability of PET-facilities with an onsite cyclotron. Thus, several non-invasive MRI-based alternatives have been proposed (Blockley et al., 2012; Pike, 2012). An easily applicable

* Corresponding author. Technical University of Munich, School of Medicine, Klinikum rechts der Isar, Department of Diagnostic and Interventional Neuroradiology, Ismaninger Str. 22, 81675, Muenchen, Germany.
E-mail address: stephan.kaczmarz@tum.de (S. Kaczmarz).

https://doi.org/10.1016/j.neuroimage.2020.117095
Received 28 February 2020; Received in revised form 11 June 2020; Accepted 18 June 2020
Available online 26 June 2020

Abbreviations

ANOVA	Analysis of variance
ASE	Asymmetric spin echo
BOLD	Blood-oxygenation-level-dependent
CBV	Cerebral blood volume
CSF	Cerebrospinal fluid
DSC	Dynamic susceptibility contrast
EHC	Elderly healthy control
EPI	Echo planar imaging
FID	Free induction decay
FLAIR	Fluid-attenuated inversion recovery
GESFIDE	Gradient Echo Sampling of FID and Echo
GESSE	Gradient Echo Sampling of Spin Echo
GM	Gray matter
GraSE	Gradient and spin echo
GRE	Gradient echo
ICAS	Internal carotid artery stenosis
MPRAGE	Magnetization prepared rapid acquisition gradient echo
mq-BOLD	Multi-parametric quantitative BOLD
MRI	Magnetic resonance imaging
NAWM	Normal appearing white matter
OEF	Oxygen extraction fraction
PET	Positron Emission Tomography
PVE	Partial volume effect
q-BOLD	Quantitative BOLD
rCBV	Relative cerebral blood volume
rOEF	Relative oxygen extraction fraction
single-SE	Single spin echo
TE	Echo time
TI	Inversion time
TR	Repetition time
TSE	Turbo spin echo
VOI	Volume of interest
WM	White matter
YHC	Young healthy control

technique with full brain coverage is multi-parametric quantitative BOLD (mq-BOLD) (Hirsch et al., 2014). This approach relies on the biophysical model of Yablonskiy and Haacke (1994) and derives relative OEF (rOEF) based on three separate measurements of transverse relaxation times by spin-echo (T_2) and gradient-echo (T_2*) as well as the relative cerebral blood volume (rCBV) (Hirsch et al., 2014). Mq-BOLD is highly promising in several pathologies, such as stroke (Gersing et al., 2015), glioma (Preibisch et al., 2017; Toth et al., 2013; Wiestler et al., 2016) and ICAS (Goettler et al., 2019; Kaczmarz et al., 2020a).

However, systematic errors still limit quantitative interpretations and impede the clinical usability of mq-BOLD. Measured rOEF = 0.6–0.7 in healthy GM was systematically elevated (Goettler et al., 2019; Kaczmarz et al., 2020b) compared to physiologically expected OEF = 0.35–0.56 (Donahue et al., 2018; Marchal et al., 1992), and was thus appropriately named relative OEF (Hirsch et al., 2014). In that regard, T_2 overestimations can occur by 2D-GraSE (**Gr**adient **a**nd **S**pin **E**cho) (Hirsch et al., 2014) as well as 2D-TSE (**T**urbo **S**pin **E**cho) imaging (Seiler et al., 2019). A known issue in T_2-mapping is stimulated echoes, which arise from imperfect matching between the excitation and refocusing pulse profiles (Hennig, 1988; Uddin et al., 2013). This is specific to 2D-acquisitions because of slice-selection pulse imperfections near slice edges. To overcome this limitation, non-slice selective (Prasloski et al., 2012a) and 3D-acquisition techniques are advisable (Prasloski et al., 2012b; Whittall et al., 1997), making 3D-GraSE (Oshio and Feinberg, 1991) ideal to overcome T_2-related bias in mq-BOLD.

The aim of this study was therefore to improve rOEF mapping by mq-BOLD towards lower, physiologically more meaningful values. We hypothesized significantly reduced T_2-related bias by applying 3D-GraSE. We further proposed a procedure to reliably identify and exclude artefact voxels to enhance the sensitivity to pathophysiological focal rOEF increases. To this end, T_2 and rOEF were compared between mq-BOLD with 2D-GraSE and 3D-GraSE in a phantom and in 25 subjects, including ICAS-patients.

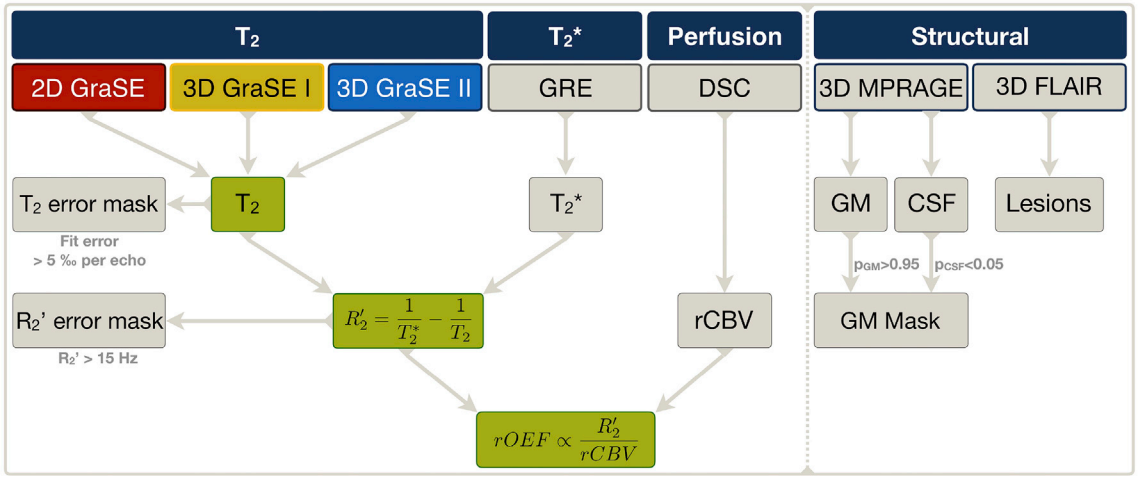

Fig. 1. Overview of applied MRI sequences and derived parameters.
The main purpose of this study was to compare the impact of three different GraSE sequences on T_2 mapping, R_2' and rOEF calculations by mq-BOLD. We therefore measured the formerly applied 2D-GraSE (red) as well as the proposed 3D-GraSE-I (yellow) and II sequences (blue). Quantitative T_2* imaging was performed by multi-echo gradient echo (GRE) imaging. R_2' was subsequently calculated from T_2 and T_2*, separately for all three GraSE sequences. Masks of elevated T_2 fit-errors (T_2 error mask) and of R_2' elevations (R_2' error mask) were generated to exclude artefact voxels. Dynamic susceptibility contrast (DSC) imaging was applied to obtain relative cerebral blood volume (rCBV) maps. By applying the mq-BOLD model to rCBV and R_2', each voxel's rOEF was calculated for each T_2 GraSE sequence, respectively. The impact of the three different GraSE sequences on T_2, R_2' and rOEF was evaluated (green). Besides, restrictive GM masks excluding CSF were generated and FLAIR lesions evaluated by structural imaging.

2. Methods

Quantitative T_2-mapping and its impact on mq-BOLD were compared for the initially applied 2D-GraSE and two proposed 3D-GraSE sequences (Fig. 1). The echo timings and scan time of 3D-GraSE-I were similar to 2D-GraSE, whereas 3D-GraSE-II used shorter echo spacing (16 ms→10 ms) with more echoes (8 → 16) and prolonged echo train (128 ms→160 ms). Evaluations were conducted in four steps. First, in a phantom compared with multiple single spin echoes (single-SE) as a reference. Second, R_2' was calculated with additionally acquired T_2*-maps in young healthy controls (YHC). In the last two steps, rOEF by mq-BOLD was evaluated in elderly healthy controls (EHC) and ICAS-patients based on the different T_2-sequences with additional T_2* and rCBV mapping.

2.1. Phantom and participants

The gel phantom contained six flasks with different T_2 relaxation times covering typical GM values (see inlay in Fig. 2B and Supplemental Table 1). For in vivo evaluations, 25 volunteers participated in this prospective study. Participants were enrolled by word-of-mouth advertisement from March until October 2017. Ten YHC (4 females, mean age 28.4 ± 4.1 years, range 21–35 years), twelve EHC (7 females, mean age 71.8 ± 5.3 years, range 63–78 years) and three patients with unilateral, high-grade, asymptomatic, extracranial ICAS were scanned (2 females, mean age 63.0 ± 9.6 years, range 52–70 years). The study was approved by the medical ethical board of the Klinikum rechts der Isar, in line with Human Research Committee guidelines of the Technical University of Munich (TUM). All participants provided informed consent in accordance with the standard protocol approvals. Data of two YHC needed to be excluded due to technical problems during data acquisition.

2.2. Image acquisition

Scanning was performed on a 3T Philips Ingenia MR-Scanner (Philips Healthcare, Best, The Netherlands) on software release R5.1.8 with a custom patch. Standard 32-channel head-receive and 16-channel head/neck-receive coils were used. The following imaging protocol was applied (see Fig. 1):

- **2D-GraSE**: 8 echoes; $TE_1 = \Delta TE = 16$ ms; TR = 8596 ms; EPI-factor = 7; α = 90°; 180° refocusing control; 30 slices; 0.3 mm gap; voxel size 2.0 × 2.1 × 3.0 mm^3; matrix 112 × 91; acq. time 2:23 min.
- **3D-GraSE-I**: 8 echoes; $TE_1 = \Delta TE = 16$ ms; TR = 251 ms; oversampling 1.3; EPI-factor = 7; TSE-factor = 8; α = 90°; 180° refocusing control; 30 slices; voxel size 2.0 × 2.1 × 3.0 mm^3; matrix 112 × 91; acq. time 2:08 min.
- **3D-GraSE-II**: 16 echoes, $TE_1 = \Delta TE = 10$ ms; TR = 487 ms; oversampling 1.3; EPI-factor = 7; TSE-factor = 16; α = 90°; 180° refocusing control; 30 slices; voxel size 2.0 × 2.1 × 3.0 mm^3; matrix 112 × 91; acq. time 4:09 min.
- **Single-SE** for phantom reference measurements: TE = 60, 70, 80, 100, 120, 140, 160 ms; TR = 3000 ms, each; 5 slices, acquired voxel size 3.5 × 4.0 × 4.0 mm^3; acq. time 2:36 min per TE.
- **Multi-echo gradient echo (GRE)**: 12 echoes, $TE_1 = \Delta TE = 5$ ms, TR = 1950 ms, α = 30°, 30 slices, matrix 112 × 92, voxel size 2.0 × 2.0 × 3.0 mm^3, total acq. time 6:08 min.
- **DSC-MRI**: single-shot GRE-EPI, 80 volumes during injection of weight-adjusted Gd-DOTA bolus (concentration 0.5 mmol/ml; dose 0.1 mmol/kg; minimum 7.5 mmol per subject; flow rate 4 ml/s) with TE = 30 ms, TR = 1513 ms; α = 60°; 26 slices; voxel size 2.0 × 2.0 × 3.5 mm^3, acq. time 2:01 min.
- **MPRAGE**: 3D acquisition, TE = 4 ms; TR = 9 ms; α = 8°; TI = 1000 ms; shot interval 2300 ms; SENSE AP/RL 1.5/2.0; 170 slices; matrix 240 × 238; voxel size 1.0 × 1.0 × 1.0 mm^3; acq. time 5:59 min

A

Sequence		T_2 in phantom flasks [ms] 1	2	3	4	5	6
Single SE		32,4 ± 1,7	48,6 ± 0,7	61,1 ± 0,9	62,6 ± 1,0	61,9 ± 0,9	105,1 ± 2,7
2D GraSE	all echoes	37,9 ± 1,2	52,5 ± 1,2	65,8 ± 1,8	68,3 ± 1,0	68,5 ± 1,4	115,7 ± 4,7
	even echoes	36,7 ± 0,9	50,9 ± 1,0	62,8 ± 1,0	64,7 ± 0,8	64,5 ± 1,0	106,2 ± 3,4
3D GraSE I		33,1 ± 1,7	45,1 ± 1,5	58,4 ± 3,3	61,6 ± 1,9	62,0 ± 2,6	101,6 ± 4,3
3D GraSE II		34,1 ± 1,6	47,1 ± 1,4	60,5 ± 2,7	63,1 ± 1,4	63,4 ± 2,1	105,1 ± 3,6

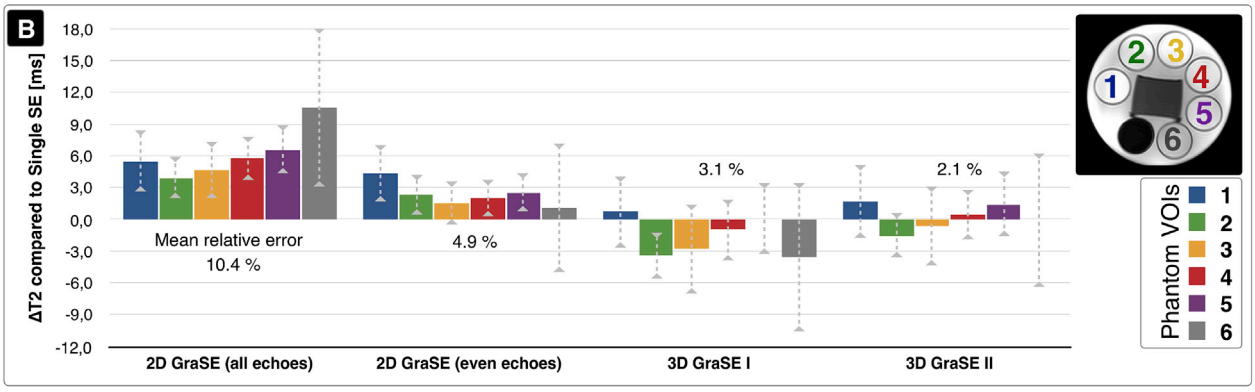

Fig. 2. Comparison of quantitative T_2 values measured by different sequences in a phantom.
The phantom contained six flasks with different T_2 relaxation times. (A) Average T_2 values within each flask are summarized for the multiple single spin echo (Single SE) reference sequence, 2D-GraSE with all and even echoes fitted, 3D-GraSE-I and 3D-GraSE-II (mean ± standard deviation) with all echoes fitted. (B) T_2 values derived from single-SE data were used as references and compared to the GraSE results. This ΔT_2 is plotted for all phantom flasks and GraSE sequences and scaled in ms. Corresponding values within each flask are shown by consistent color coding (see inlay in B). The average T_2 deviation of each GraSE sequence is noted in percent. Best accordance was found for 3D-GraSE-II.

- **FLAIR**: 3D acquisition, TE = 289 ms; TR = 4800 ms; TI = 1650 ms; α = 90°; TSE-factor = 167; 163 slices; matrix 224 × 224; voxel size 1.1 × 1.1 × 1.1 mm^3; acq. time 4:34 min.

2.3. Image analysis

Data evaluations were performed using MATLAB R2016b (The MathWorks Inc., Natick, USA) and SPM12 (v6225) (Penny et al., 2011) with custom programs. Quantitative T_2 parameter maps were derived by mono-exponential fittings of all echoes for 3D-GraSE and only even echoes for 2D-GraSE in vivo, as initially implemented to reduce stimulated echoes (Hirsch et al., 2014). Multi-echo GRE data were corrected for macroscopic background gradients (Baudrexel et al., 2009; Hirsch and Preibisch, 2013) and motion (Magerkurth et al., 2011) before mono-exponential fitting for T_2* and spatial coregistration to T_2. Both, T_2* and T_2-maps were smoothed with a 3D Gaussian filter-kernel of 3 mm prior to the calculation of

$$R_2' = \frac{1}{T_2^*} - \frac{1}{T_2}. \quad [1]$$

DSC data was processed as described previously (Hedderich et al., 2019; Kluge et al., 2016) with CBV normalization to 2.5% in normal appearing white matter (NAWM) (Leenders, 1994), yielding relative CBV (rCBV). Following the mq-BOLD approach, rOEF was calculated as

$$rOEF = \frac{R_2'}{c \cdot rCBV} \quad [2]$$

with $c = \gamma \cdot \frac{4}{3} \cdot \pi \cdot \Delta\chi \cdot B_0, B_0 = 3T$ and $\Delta\chi = \mathrm{Hct} \cdot \Delta\chi_0 = 0.35 \cdot 0.264 \cdot 10^{-6} = 0.924 \cdot 10^{-7}$ (Hirsch et al., 2014).

To investigate the impact of the different T_2-mapping sequences, R_2' and rOEF were calculated with the same T_2* and rCBV (Fig. 1). For quality assessment, all parameter maps were screened specifically for motion artefacts and spatial misregistration (raters: SK, CP).

2.4. Artefact removal

To account for mismatches between the measured data and mono-exponential fittings of T_2 and T_2*, fit-errors were evaluated on a voxel-wise basis and normalized by the number of acquired echoes. Empirically set thresholds were applied and checked carefully (SK, CP). Voxels with fit-errors>5‰ per echo were excluded from data evaluation (Supplemental Fig. 1). An additional threshold of $R_2' < 15\ s^{-1}$ was applied (Kaczmarz et al., 2020b) to exclude areas with iron-induced focal R_2' increases, especially in deep GM regions. This also excluded areas with higher macroscopic background gradients, as corrections are only reliable up to approximately 220 μT/m (Hirsch and Preibisch, 2013).

2.5. Statistical analyses

Phantom measurements were evaluated by averaging T_2-values within VOIs in each flask. 2D-GraSE was compared with 3D-GraSE-I, II and single-SE reference values (Prasloski et al., 2012b). For in-vivo evaluations, restrictive GM masks were generated from MPRAGE segmentations ($p_{GM}>0.95$) with additional CSF exclusion ($p_{CSF}<0.05$). Within these masks, average T_2, T_2*, R_2', rCBV, and rOEF values were calculated. The impact of 2D vs. 3D-GraSE on T_2, R_2' and rOEF values in GM on group level was illustrated by paired scatter plots. Significance of group mean value differences was tested by ANOVA, homogeneity of variance asserted using Levene's test and pairwise correlations corrected for multiple comparisons with Tukey or Games-Howell post-hoc analysis in SPSS (v26, IBM Corp., Armonk, USA). Values of $p < 0.05$ were considered statistically significant. Distributions of the fit-errors and parameter values were compared by histograms.

3. Results

In the phantom, single-SE reference measurements revealed average transverse T_2 relaxation times between 32.4 and 105.1 ms within the six flasks. By comparison, the original 2D-GraSE sequence overestimated T_2 by 10.4% with all echo fitting and 4.9% with even echoes only. The 3D-GraSE-I and II sequences reduced overestimations to 3.1% and 2.1%, respectively (Fig. 2).

In YHC, quantitative T_2-mapping by 2D-GraSE with even echo fitting yielded $T_2 = 83.9 \pm 1.1$ ms. 3D-GraSE-I and II decreased T_2 by −8.8% and −6.8%, respectively ($T_2 = 76.5 \pm 1.2$ ms and 78.2 ± 1.1 ms; $p < 0.001$, each). Consequently, R_2' decreased by −14.5% and −13.3% for 3D-GraSE-I and II ($R_2' = 6.9 \pm 0.3\ s^{-1}$ and $7.2 \pm 0.4\ s^{-1}$) compared to $R_2' = 8.3 \pm 0.4\ s^{-1}$ by 2D-GraSE with $T_2^* = 53.9 \pm 1.7$ ms (Table 1). Additional artefact exclusion further reduced the T_2 and R_2' values (3D-GraSE-I: $T_2 = 75.2 \pm 1.0$ ms and $R_2' = 5.6 \pm 0.2\ s^{-1}$; 3D-GraSE-II: $T_2 = 77.9 \pm 1.0$ ms and $R_2' = 6.1 \pm 0.2\ s^{-1}$). While artefact exclusion effects on T_2-values were comparably weak ($p > 0.5$; Fig. 3A), R_2' values decreased by up to −32.5% ($p < 0.001$; Fig. 3B). Fit-errors of 3D-GraSE-II were much lower (0.1%) compared to 3D-GraSE-I (19.6%) and 2D-GraSE (15.3%, Fig. 3C; Table 2). For 3D-GraSE-II, most excluded voxels were affected by T_2* fit-errors (83.3%), followed by R_2' elevations (51.5%) and only minor T_2 fit-errors (0.9%). The fraction of voxels in GM excluded due to R_2' thresholding was similar between 2D (9.7%) and 3D-GraSE-II (7.3%). Due to lowest errors and time restrictions, 3D-GraSE-II was applied in the following evaluations in EHC as well as ICAS-patients and compared with 2D-GraSE.

In EHC, 2D-GraSE yielded T_2-values of 89.2 ± 3.1 ms. Average GM values of $R_2' = 8.5 \pm 0.7\ s^{-1}$ and rOEF = 0.70 ± 0.08 were calculated from additional measurements of T_2* (55.7 ± 4.0 ms) and rCBV (4.71 ± 0.27%) (Table 1). The application of 3D-GraSE-II significantly decreased T_2 by −8.5% ($T_2 = 81.6 \pm 1.9$ ms; $p < 0.001$), R_2' by −12.9% ($R_2' = 7.4 \pm 0.7\ s^{-1}$, $p < 0.001$) and rOEF by −15.7% (rOEF = 0.59 ± 0.08, $p < 0.03$). Artefact exclusion further decreased R_2' and rOEF by up to −27.1% in total ($R_2' = 6.6 \pm 0.6\ s^{-1}$; rOEF = 0.51 ± 0.06; $p < 0.03$; Fig. 4). FLAIR lesion gradings with an average Fazekas-score of 1.3 indicated only minor microangiopathic changes (Fazekas et al., 1987). None of the participants had subacute or older territorial infarct lesions.

In ICAS, all parameter values decreased with 3D-GraSE-II and artefact exclusion, yielding similar values as in EHC (Table 1). Furthermore, focal rOEF hyperintensities ipsilateral to the stenosis were enhanced and only recognizable by 3D-GraSE-II (Fig. 5A). Two regions stand out in the artefact maps. First, well-known iron deposition in the striatum corresponds to maximum rOEF-values. Second, artefact voxels occur along the brains' surface towards the cranial bone (Fig. 5A). Artefact removal in 3D-GraSE-II improved rOEF towards lower values and additionally decreased the number of voxels with maximum rOEF values (Fig. 5B).

4. Discussion

T_2-mapping by 2D-vs 3D-GraSE was compared with regard to their impact on rOEF values modeled by mq-BOLD. Formerly overestimated T_2, R_2' and rOEF values significantly improved by 3D-GraSE, as hypothesized. Remarkably, 3D-GraSE-II also improved the fit quality, lowering the number of excluded artefact voxels due to T_2 fit-errors in ICAS-patients by the factor 30. The specific impact of 3D-GraSE on T_2, R_2' and rOEF are discussed below.

4.1. Impact on T_2

The phantom measurements confirmed T_2 overestimations by 2D-GraSE (Hirsch et al., 2014). 3D-GraSE lowered T_2-values, as hypothesized, only deviating 2.1% from single-SE values. Similarly, comparisons in YHC confirmed overestimations by 2D-GraSE, whereas lower average GM values of $T_2 = 76.5$ ms were measured with 3D-GraSE-I. This agrees well with literature values at 3T of $T_2 = 73.5$ ms in YHC by single-SE

Table 1
Summary of average parameter values for all groups.
Quantitative parameter values were compared for YHC, EHC and ICAS-patients. The number of scanned participants is shown for each group. Two YHC were excluded due to data acquisitions problems. Average T_2 values in GM were calculated for all GraSE sequences (group mean ± standard deviation), each with and without artefact exclusion ("corrected"). Displayed 2D-GraSE values were generated by fitting of even echoes only. Resulting R_2' values were calculated from GraSE-based T_2 values and GRE-based T_2*. For EHC and ICAS-patients, rOEF values were calculated from R_2' and additionally acquired DSC-based rCBV maps. Note, 3D-GraSE-I and II decreased T_2, R_2' and rOEF towards physiologically more realistic values for all subject groups.

Participants	Average T2 in GM [ms]						
Group	n	2D GraSE	2D GraSE corrected	3D GraSE I	3D GraSE I corrected	3D GraSE II	3D GraSE II corrected
YHC	10	83.9 ± 1.1	81.6 ± 0.9	76.5 ± 1.2	75.2 ± 1.0	78.2 ± 1.1	77.9 ± 1.0
EHC	12	89.2 ± 3.1	85.4 ± 2.5	–	–	81.6 ± 1.9	81.2 ± 2.0
ICAS	3	89.6 ± 1.3	85.9 ± 1.8	–	–	82.9 ± 0.7	82.2 ± 1.2

Participants	**Average R2' in GM [1/s]**							**T2* [ms]**
Group	n	2D GraSE	2D GraSE corrected	3D GraSE I	3D GraSE I corrected	3D GraSE II	3D GraSE II corrected	
YHC	10	8.3 ± 0.4	6.9 ± 0.3	6.9 ± 0.3	5.6 ± 0.2	7.2 ± 0.4	6.1 ± 0.2	53.9 ± 1.7
EHC	12	8.5 ± 0.7	7.7 ± 0.6	–	–	7.4 ± 0.7	6.6 ± 0.6	55.7 ± 4.0
ICAS	3	8.4 ± 0.7	7.3 ± 0.4	–	–	7.6 ± 0.9	6.6 ± 0.5	56.5 ± 2.4

Participants	**Average rOEF in GM []**							**rCBV [%]**
Group	**n**	**2D GraSE**	**2D GraSE corrected**	**3D GraSE I**	**3D GraSE I corrected**	**3D GraSE II**	**3D GraSE II corrected**	
YHC	10	–	–	–	–	–	–	–
EHC	12	0.70 ± 0.08	0.61 ± 0.06	–	–	0.59 ± 0.08	0.51 ± 0.06	4.71 ± 0.27
ICAS	3	0.65 ± 0.05	0.59 ± 0.02	–	–	0.58 ± 0.06	0.52 ± 0.03	4.68 ± 0.04

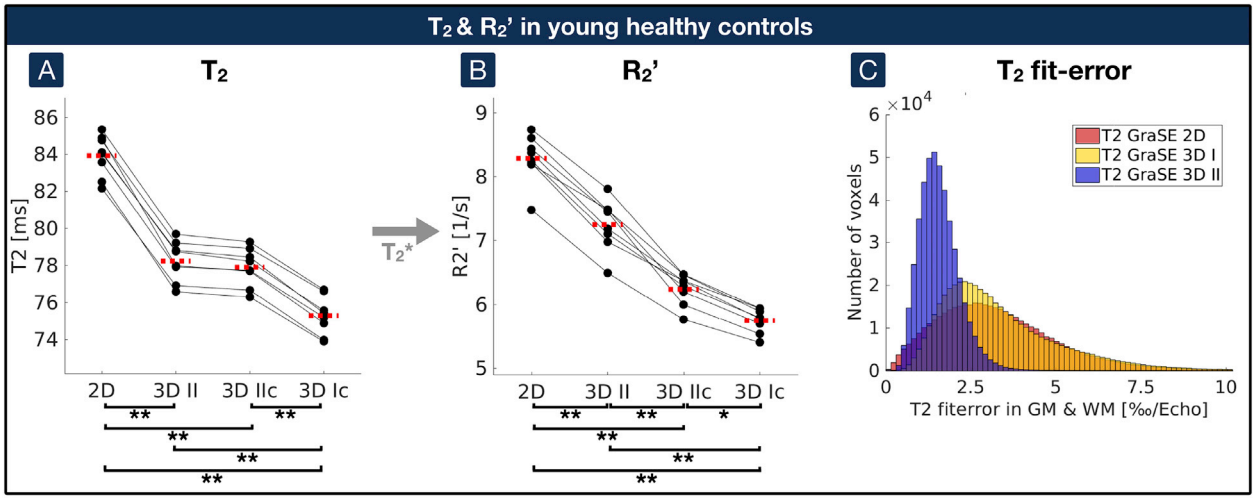

Fig. 3. Impact of GraSE sequences and artefact exclusion on T_2 and R_2' compared by paired scatterplots in young healthy controls.
(A) Quantitative T_2 values in GM were compared between the 2D-GraSE ("2D"), 3D-GraSE-II ("3D II"), 3D-GraSE-II with additional artefact exclusion ("3D IIc") and 3D-GraSE-I with artefact exclusion ("3D Ic"). Voxels with elevated T_2 fit-errors or R_2' elevations were excluded by artefact exclusion. (B) R_2' was calculated based on T_2 values from the different GraSE sequences with the same quantitative T_2* map. (A, B) Single participant's average parameter values in GM are represented by black dots. Corresponding values of the same participant are connected by black lines. Median values on group level are indicated by red dashed lines for each parameter and acquisition technique. Asterisks indicate significant differences with $p < 0.03$, double asterisks $p < 0.001$ with correction for multiple comparisons. (C) Errors of the T_2 fits were compared for the three GraSE sequences. Average errors within GM of all participants are shown in the histogram. Voxels with fit-errors > 5‰ per echo were excluded from the artefact-corrected analyses ("3D Ic" and "3D IIc"). Note much lower fit-errors in 3D-GraSE-II, indicating better fitting quality (blue).

(Hirsch et al., 2014) and $T_2 = 76.2$ ms in EHC by multi-SE (Christen et al., 2012). The proposed artefact voxel exclusion further improved T_2-values. While both 3D-GraSE sequences improved T_2, 3D-GraSE-II performed best with regards to lowest fit errors, due to its improved echo sampling. Evaluations of average fit-errors revealed improvements in 3D-GraSE vs. 2D-GraSE by a factor up to 2 (Supplemental Fig. 2) and reduced voxel exclusions due to T_2 fit-errors up 150 times (Table 2).

Literature values of alternative T_2-mapping by TSE yielded much higher healthy average GM values of 119 ms (Sedlacik et al., 2014; Wagner et al., 2012, 2015), which necessitates sophisticated quantitative T_2 post-processing corrections (Noth et al., 2017). Thus, 3D-GraSE is ideal for fast, quantitative T_2-mapping with full brain coverage (Prasloski et al., 2012b; Whittall et al., 1997).

4.2. Impact on R_2'

R_2' was calculated based on T_2 and additional T_2*-mapping. As for T_2, average R_2' values decreased with 3D-GraSE to $R_2' = 6.1\ s^{-1}$ in YHC, with artefact exclusion. This is in good agreement with literature values by GRE and TSE of similar aged healthy participants in frontal cortex with $R_2' = 7.4\ s^{-1}$ (Sedlacik et al., 2014) and $R_2' = 7.9\ s^{-1}$ (Wagner et al., 2012). Remaining deviations may be due to fittings of only 3 and 5 echoes for T_2 in those studies, respectively, which might be insufficient (Whittall et al., 1997). In general, reported average R_2' values vary. While much higher average GM values of $R_2' = 12.0\ s^{-1}$ have been reported by GRE and TSE (Wagner et al., 2015), other methods reported lower values, specifically $R_2' = 5.1\ s^{-1}$ by GRE (Ulrich and Yablonskiy,

Table 2
Summary of average fit-errors for all groups.
Fit-errors were compared for YHC, EHC and ICAS-patients. The number of scanned participants is shown for each group. Fit-errors in GM were evaluated for the 2D-GraSE, 3D-GraSE-I and 3D-GraSE-II, scaled in permille per echo (group mean ± standard deviation). Voxels with fit-errors>5‰ per echo were excluded. The corresponding fraction of excluded GM voxels due to T_2 fit-errors are compared for all sequences and groups. Note, clearly decreased errors by 3D-GraSE-II with only few excluded voxels (≤1%).

Participants		Average T2 fit-error in GM [‰/echo]			Fraction of excluded GM voxels (with error > 5‰/echo) [%]		
Group	n	2D GraSE	3D GraSE I	3D GraSE II	2D GraSE	3D GraSE I	3D GraSE II
YHC	10	3.2 ± 0.2	3.5 ± 0.3	1.5 ± 0.1	15.3	19.6	0.1
EHC	12	4.0 ± 0.3	–	1.8 ± 0.1	26.4	–	0.3
ICAS	3	4.0 ± 0.2	–	1.8 ± 0.2	28.4	–	1.0

2015), $R_2' = 3.0\ s^{-1}$ and $4.4\ s^{-1}$ by asymmetric spin echo (ASE) (An and Lin, 2003; Blockley and Stone, 2016), $R_2' = 2.9\ s^{-1}$ by GESSE (He and Yablonskiy, 2007) and $R_2' = 2.7\ s^{-1}$ by Gradient Echo Sampling of FID and Echo (GESFIDE) (Ni et al., 2014).

The proposed artefact exclusion had stronger effects on average R_2' than T_2 values, due to removal of R_2' elevations, which were caused by strong susceptibility gradients at the borders and in fronto-basal and temporal brain regions as well as iron deposition in the striatum (Fig. 5A and Supplemental Fig. 3). As R_2' values decreased with 3D-GraSE-II compared to 2D-GraSE, slightly fewer voxels were excluded by R_2' thresholding. Iron concentration increases with age could explain increased number of artefact voxels in EHC vs. YHC. The observed R_2' increases with age also agree with literature (Sedlacik et al., 2014).

4.3. Impact on rOEF

Maps of rOEF were calculated in EHC and ICAS-patients based on R_2' and additional rCBV measurements. 2D-GraSE yielded rOEF = 0.70 in accordance with previously reported overestimations (Hirsch et al., 2014). But rOEF was significantly lower with 3D-GraSE. Artefact exclusion further decreased the average GM value to rOEF = 0.51 in EHC. Overall, rOEF values decreased by −27.1% by 3D-GraSE and artefact exclusion, which is more similar to literature values from PET measurements (Donahue et al., 2018; Marchal et al., 1992). While a similar mq-BOLD implementation using the same model yielded much lower average OEF = 0.33 in healthy controls (Christen et al., 2012), they restricted T_2 imaging echo-times to maximum 55 ms. Together with comparably high CBV values, this explains their systematically lower OEF values (see Eqs. (1) and (2)).

Values of T_2, R_2' and rOEF with 3D-GraSE were comparable in EHC and ICAS-patients. This is in line with previously observed unaffected rOEF on group level in high-grade stenosis patients (Bouvier et al., 2015; Goettler et al., 2019). Nevertheless, focal rOEF increases have been found (Kaczmarz et al., 2020a), which potentially have a high clinical relevance as an indicator of misery perfusion to assess individual stroke risks (Baron et al., 1981). Interestingly, those focal rOEF elevations were only visible with 3D-GraSE (Fig. 5A). Pathophysiological origins of rOEF elevations are supported by their localization at the border zone between perfusion territories (Supplemental Fig. 4), measured by super-selective arterial spin labeling (Helle et al., 2010). This increased sensitivity of mq-BOLD with 3D-GraSE in an ICAS-patient, as a proof-of-principle, is highly promising for the detection of even subtle oxygenation changes.

4.4. Applicability and limitations

An obvious strength of this study is its potential for widespread clinical applications due to standard sequences. Minor remaining T_2 variations may be attributed to diffusion effects, especially for single-SE (Carr and Purcell, 1954), and known echo timing dependencies, which are also related to diffusion (Poon and Henkelman, 1992; Whittall et al., 1999). In vivo scans can be additionally affected by partial volume effects (PVE), especially in presence of CSF contamination (Whittall et al., 1999), and multi-compartmental tissue structures (MacKay et al., 2006). Nevertheless, mono-exponential fittings were applied to achieve full brain volume coverage within clinically feasible scan times, while multi-exponential fittings would require higher SNR (Whittall et al., 1997).

Measured rOEF values may be slightly higher than literature PET values due to PVE, especially with CSF (He and Yablonskiy, 2007; Stone

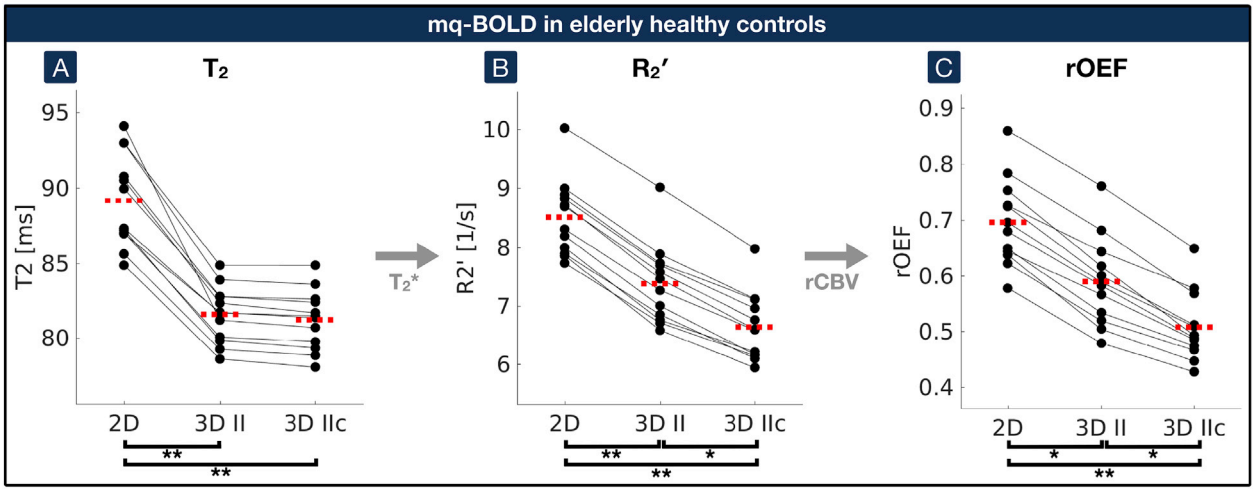

Fig. 4. Impact of 2D and 3D-GraSE-II sequences on mq-BOLD parameters by paired scatterplots in elderly healthy controls.
(A) Quantitative T_2-values acquired by 2D-GraSE ("2D"), 3D-GraSE-II ("3D II") and with additional artefact correction ("3D IIc") were compared. (B) R_2' was calculated based on T_2 values obtained by the different GraSE sequences and the quantitative T_2*-map. (C) R_2' values were combined with DSC-based rCBV to calculate rOEF according to the mq-BOLD model. Single participant's average parameter values in GM are represented by black dots. Corresponding values of the same participant are connected by black lines. Median values on group level are indicated by red dashed lines for each parameter and sequence. Asterisks indicate significant differences with $p < 0.03$, double asterisks $p < 0.001$ with correction for multiple comparisons. While artefact correction of 3D-GraSE ("3D IIc") has a comparably low impact on T_2, corresponding R_2' and rOEF values were significantly decreased.

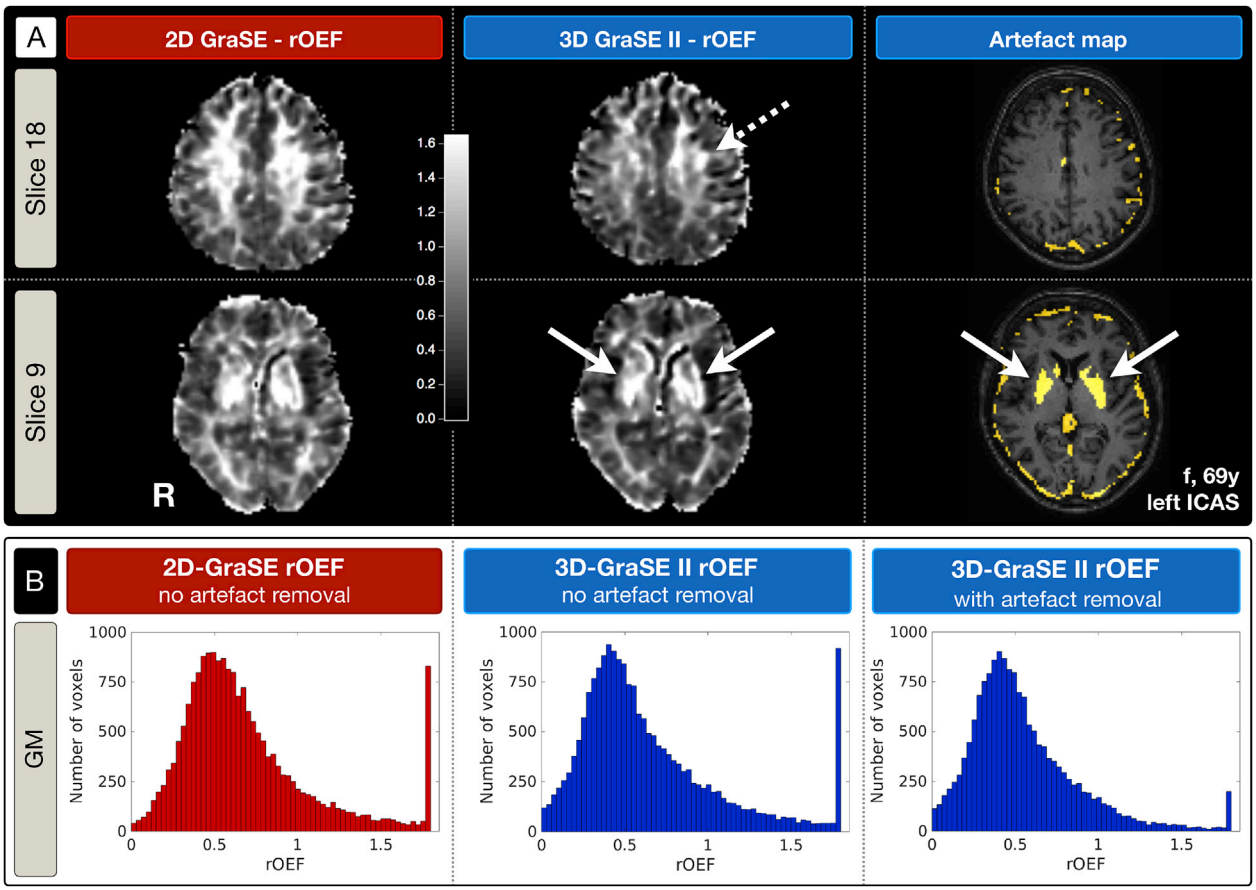

Fig. 5. Exemplary rOEF and artefact maps of a left-sided ICAS-patient comparing 2D-GraSE vs. 3D-GraSE-II.
(A) rOEF-maps derived by 2D-GraSE (indicated in red) vs. 3D-GraSE-II (blue) and the corresponding artefact map of 3D-GraSE-II are compared in two axial slices. All rOEF-maps are displayed within the same colormap scaling (0 to 1.6). Note that focal rOEF hyperintensities ipsilateral to the stenosis, potentially related to patho-physiological effects, are located at the perfusion territories border zone (Supplemental Fig. 4) and only apparent by 3D-Grase-II based rOEF (dashed arrow). Artefact voxels with elevated fitting errors of T_2 and T_2* or R_2' increases are shown in yellow. The striatum with high-iron content is clearly visible in the artefact-map and corresponds to maximum rOEF values (solid arrows). (B) rOEF value distributions are compared by histograms. They highlight the lower rOEF values by 3D-GraSE-II compared to 2D-GraSE. Moreover, additional artefact removal of 3D-GraSE-II reduced the frequency of maximum values of rOEF = 1.8.

and Blockley, 2017). Smoothing may further enhance those effects, but was applied as spatial resolutions of the sequences were only harmonized as far as possible, while maintaining parameters of standard clinical protocols. Those effects were accounted for by restrictive GM thresholding and CSF exclusion.

Furthermore, the mq-BOLD implementation neglects intravascular signals (Hirsch et al., 2014; Yablonskiy and Haacke, 1994), even though effects on T_2* might be non-negligible at 3T (Donahue et al., 2011; Li and van Zijl, 2020). While profound investigations based on a recent model (Berman and Pike, 2018) found minor intravascular effects on q-BOLD parameter estimates in ASE, intravascular effects were demonstrated in simulations of a GESSE sequence (Stone et al., 2019). Thus, future consideration of intravascular signal contributions in mq-BOLD may be beneficial (He and Yablonskiy, 2007). Other potential confounders are neglects of vessel size dependent hematocrit variations and imperfect SE refocusing (Berman et al., 2018). While 3D-GraSE lowered whole brain rOEF values (Fig. 5A), evaluations were restricted to GM due to known artefactual GM-WM rOEF contrast, mainly caused by approximating venous CBV by total rCBV (Hirsch et al., 2014) and, although minor on average, vessel orientation effects in WM (Kaczmarz et al., 2020b). CBV normalization to NAWM might limit sensitivity to global differences between subjects, groups and in longitudinal studies. While the threshold of $R_2' < 15\ s^{-1}$ was applied based on previous work, lower thresholds, in general, directly result in lower average rOEF values. Thus, excluded voxels were carefully evaluated to avoid potential confounds.

4.5. Outlook

The presented improvements by 3D-GraSE are also highly promising for R_2'-based calibrated BOLD measurements as a viable alternative to complex gas challenges (He and Yablonskiy, 2007; Kida et al., 2000; Liu et al., 2019; Shu et al., 2016a). Physiological underpinnings of the BOLD signal could hereby be measured in activation studies (Blockley et al., 2012).

5. Conclusions

We demonstrated the successful implementation of 3D-GraSE-based T_2-imaging in mq-BOLD for whole brain rOEF mapping within clinically applicable scan times. Measured T_2 values with 3D-GraSE were in excellent agreement with the literature. With additional artefact exclusion, formerly overestimated rOEF decreased up to −27%. Measured average rOEF = 0.51 in GM is considerably closer to literature values. Interestingly, focal rOEF increases in an ICAS-patient only became apparent by 3D-GraSE, which shows great promise for future clinical applications of mq-BOLD.

Data and code availability

For reasons of ethics and privacy issues of the acquired clinical data, the data is only available via a request to the authors.

Institutional restrictions of patient privacy then require a formal data sharing agreement. The applied MATLAB code is available upon request. Sharing of applied sequence modifications is limited by a non-disclosure agreement. The applied sequence changes have been published (Hirsch and Preibisch, 2013) and further information will be shared on request. Custom MATLAB code for post-processing of mq-BOLD MRI data for neuro-scientific studies is available at https://doi.org/10.5281/zenodo.3909300 and https://gitlab.lrz.de/nmrm_lab/public_projects/mq-BOLD.

Declaration of conflicting interest

The authors declared no potential conflicts of interest with respect to the research, authorship, and/or publication of this article.

CRediT authorship contribution statement

Stephan Kaczmarz: Funding acquisition, Formal analysis, Writing - original draft. **Fahmeed Hyder:** Writing - review & editing. **Christine Preibisch:** Supervision, Writing - review & editing.

Acknowledgments

We would like to thank Dr. Jens Göttler, Dr. Nico Sollmann and Ilias Tsiachristos for their support in participant recruitment and during the MRI measurements. We are very grateful to Dr. Andreas Hock from Philips Healthcare for his support regarding the MR-sequences and PD Dr. Michael Helle, also from Philips Healthcare, for his support on the perfusion territory mapping. We also thank Prof. Dr. Ralf Deichmann from the Goethe University in Frankfurt/Main for his support to correct T_2* parameter maps for motion and macroscopic background gradients. We thank all our study participants for their efforts to take part in this study.

This work was supported by the Friedrich-Ebert-Stiftung (grant to SK), the Dr.-Ing. Leonhard Lorenz-Stiftung (grant to SK 971/19) and the German Research Foundation (DFG) – Project number PR 1039/6-1 (grant to CP). FH was supported by NIH grants (R01 MH-067528, R01 NS-100106, P30 NS-052519).

Appendix A. Supplementary data

Supplementary data to this article can be found online at https://doi.org/10.1016/j.neuroimage.2020.117095.

References

An, H., Lin, W., 2003. Impact of intravascular signal on quantitative measures of cerebral oxygen extraction and blood volume under normo- and hypercapnic conditions using an asymmetric spin echo approach. Magn. Reson. Med. 50, 708–716.

Baron, J.C., Bousser, M.G., Rey, A., Guillard, A., Comar, D., Castaigne, P., 1981. Reversal of focal misery-perfusion syndrome by extra-intracranial arterial bypass in hemodynamic cerebral ischemia. A case study with 15O positron emission tomography. Stroke 12, 454–459.

Baudrexel, S., Volz, S., Preibisch, C., Klein, J.C., Steinmetz, H., Hilker, R., Deichmann, R., 2009. Rapid single-scan T 2*-mapping using exponential excitation pulses and image-based correction for linear background gradients. Magn. Reson. Med. 62, 263–268.

Berman, A.J.L., Mazerolle, E.L., MacDonald, M.E., Blockley, N.P., Luh, W.M., Pike, G.B., 2018. Gas-free calibrated fMRI with a correction for vessel-size sensitivity. Neuroimage 169, 176–188.

Berman, A.J.L., Pike, G.B., 2018. Transverse signal decay under the weak field approximation: theory and validation. Magn. Reson. Med. 80, 341–350.

Blockley, N.P., Griffeth, V.E.M., Buxton, R.B., 2012. A general analysis of calibrated BOLD methodology for measuring CMRO(2) responses: comparison of a new approach with existing methods. Neuroimage 60, 279–289.

Blockley, N.P., Stone, A.J., 2016. Improving the specificity of R2′ to the deoxyhaemoglobin content of brain tissue: prospective correction of macroscopic magnetic field gradients. Neuroimage 135, 253–260.

Bouvier, J., Detante, O., Tahon, F., Attye, A., Perret, T., Chechin, D., Barbieux, M., Boubagra, K., Garambois, K., Tropres, I., Grand, S., Barbier, E.L., Krainik, A., 2015. Reduced CMRO2 and cerebrovascular reserve in patients with severe intracranial arterial stenosis: a combined multiparametric qBOLD oxygenation and BOLD fMRI study. Hum. Brain Mapp. 36, 695–706.

Carr, H.Y., Purcell, E.M., 1954. Effects of diffusion on free precession in nuclear magnetic resonance experiments. Phys. Rev. 94, 630–638.

Christen, T., Schmiedeskamp, H., Straka, M., Bammer, R., Zaharchuk, G., 2012. Measuring brain oxygenation in humans using a multiparametric quantitative blood oxygenation level dependent MRI approach. Magn. Reson. Med. 68, 905–911.

Derdeyn, C.P., Videen, T.O., Yundt, K.D., Fritsch, S.M., Carpenter, D.A., Grubb, R.L., Powers, W.J., 2002. Variability of cerebral blood volume and oxygen extraction: stages of cerebral haemodynamic impairment revisited. Brain 125, 595–607.

Donahue, M.J., Achten, E., Cogswell, P.M., De Leeuw, F.E., Derdeyn, C.P., Dijkhuizen, R.M., Fan, A.P., Ghaznawi, R., Heit, J.J., Ikram, M.A., Jezzard, P., Jordan, L.C., Jouvent, E., Knutsson, L., Leigh, R., Liebeskind, D.S., Lin, W., Okell, T.W., Qureshi, A.I., Stagg, C.J., van Osch, M.J., van Zijl, P.C., Watchmaker, J.M., Wintermark, M., Wu, O., Zaharchuk, G., Zhou, J., Hendrikse, J., 2018. Consensus statement on current and emerging methods for the diagnosis and evaluation of cerebrovascular disease. J. Cerebr. Blood Flow Metabol. 38, 1391–1417.

Donahue, M.J., Hoogduin, H., van Zijl, P.C., Jezzard, P., Luijten, P.R., Hendrikse, J., 2011. Blood oxygenation level-dependent (BOLD) total and extravascular signal changes and DeltaR2* in human visual cortex at 1.5, 3.0 and 7.0 T. NMR Biomed. 24, 25–34.

Epp, S., Preibisch, C., Andrews-Hanna, J., Riedl, V., 2019. Towards a Metabolic Baseline for Default Mode Network Activations and Deactivations. OHBM, Rome, Italy.

Fazekas, F., Chawluk, J.B., Alavi, A., Hurtig, H.I., Zimmerman, R.A., 1987. MR signal abnormalities at 1.5 T in Alzheimer's dementia and normal aging. AJR Am. J. Roentgenol. 149, 351–356.

Gersing, A.S., Ankenbrank, M., Schwaiger, B.J., Toth, V., Janssen, I., Kooijman, H., Wunderlich, S., Bauer, J.S., Zimmer, C., Preibisch, C., 2015. Mapping of cerebral metabolic rate of oxygen using dynamic susceptibility contrast and blood oxygen level dependent MR imaging in acute ischemic stroke. Neuroradiology 57, 1253–1261.

Goettler, J., Kaczmarz, S., Kallmayer, M., Wustrow, I., Eckstein, H.H., Zimmer, C., Sorg, C., Preibisch, C., Hyder, F., 2019. Flow-metabolism uncoupling in patients with asymptomatic unilateral carotid artery stenosis assessed by multi-modal magnetic resonance imaging. J. Cerebr. Blood Flow Metabol. 39, 2132–2143.

He, X., Yablonskiy, D.A., 2007. Quantitative BOLD: mapping of human cerebral deoxygenated blood volume and oxygen extraction fraction: default state. Magn. Reson. Med. 57, 115–126.

Hedderich, D., Kluge, A., Pyka, T., Zimmer, C., Kirschke, J.S., Wiestler, B., Preibisch, C., 2019. Consistency of normalized cerebral blood volume values in glioblastoma using different leakage correction algorithms on dynamic susceptibility contrast magnetic resonance imaging data without and with prebolus. J. Neuroradiol. 46 (1), 44–51.

Helle, M., Norris, D.G., Rüfer, S., Alfke, K., Jansen, O., van Osch, M.J.P., 2010. Superselective pseudocontinuous arterial spin labeling. Magn. Reson. Med. 64, 777–786.

Hennig, J., 1988. Multiecho imaging sequences with low refocusing flip angles. J. Magn. Reson. 78, 397–407, 1969.

Hirsch, N.M., Preibisch, C., 2013. T2* mapping with background gradient correction using different excitation pulse shapes. AJNR Am. J. Neuroradiol. 34, E65–E68.

Hirsch, N.M., Toth, V., Forschler, A., Kooijman, H., Zimmer, C., Preibisch, C., 2014. Technical considerations on the validity of blood oxygenation level-dependent-based MR assessment of vascular deoxygenation. NMR Biomed. 27, 853–862.

Hyder, F., 2009. Dynamic imaging of brain function. Methods Mol. Biol. 489, 3–21.

Hyder, F., Rothman, D.L., Shulman, R.G., 2002. Total neuroenergetics support localized brain activity: implications for the interpretation of fMRI. Proc. Natl. Acad. Sci. U. S. A. 99, 10771–10776.

Kaczmarz, S., Gottler, J., Petr, J., Hansen, M.B., Mouridsen, K., Zimmer, C., Hyder, F., Preibisch, C., 2020a. Hemodynamic impairments within individual watershed areas in asymptomatic carotid artery stenosis by multimodal MRI. J. Cerebr. Blood Flow Metabol. 271678x20912364.

Kaczmarz, S., Gottler, J., Zimmer, C., Hyder, F., Preibisch, C., 2020b. Characterizing white matter fiber orientation effects on multi-parametric quantitative BOLD assessment of oxygen extraction fraction. J. Cerebr. Blood Flow Metabol. 40, 760–774.

Kida, I., Kennan, R.P., Rothman, D.L., Behar, K.L., Hyder, F., 2000. High-resolution CMRO2 mapping in rat cortex: a multiparametric approach to calibration of BOLD image contrast at 7 tesla. J. Cerebr. Blood Flow Metabol. 20, 847–860.

Kluge, A., Lukas, M., Toth, V., Pyka, T., Zimmer, C., Preibisch, C., 2016. Analysis of three leakage-correction methods for DSC-based measurement of relative cerebral blood volume with respect to heterogeneity in human gliomas. Magn. Reson. Imaging 34, 410–421.

Leenders, K.L., 1994. PET: blood flow and oxygen consumption in brain tumors. J. Neuro Oncol. 22, 269–273.

Li, W., van Zijl, P.C.M., 2020. Quantitative theory for the transverse relaxation time of blood water. NMR Biomed. 33, e4207.

Liu, E.Y., Guo, J., Simon, A.B., Haist, F., Dubowitz, D.J., Buxton, R.B., 2019. The potential for gas-free measurements of absolute oxygen metabolism during both baseline and activation states in the human brain. Neuroimage, 116342.

MacKay, A., Laule, C., Vavasour, I., Bjarnason, T., Kolind, S., Mädler, B., 2006. Insights into brain microstructure from the T2 distribution. Magn. Reson. Imag. 24, 515–525.

Magerkurth, J., Volz, S., Wagner, M., Jurcoane, A., Anti, S., Seiler, A., Hattingen, E., Deichmann, R., 2011. Quantitative T*2-mapping based on multi-slice multiple gradient echo flash imaging: retrospective correction for subject motion effects. Magn. Reson. Med. 66, 989–997.

Marchal, G., Rioux, P., Petit-Taboué, M.-C., Sette, G., Travère, J.-M., Le Poec, C., Courtheoux, P., Derlon, J.-M., Baron, J.-C., 1992. Regional cerebral oxygen consumption, blood flow, and blood volume in healthy human aging. Arch. Neurol. 49, 1013–1020.

Ni, W., Christen, T., Zun, Z., Zaharchuk, G., 2014. Comparison of R2′ measurement methods in the normal brain at 3 tesla. Magn. Reson. Med. 73, 1228–1236.
Noth, U., Shrestha, M., Schure, J.R., Deichmann, R., 2017. Quantitative in vivo T2 mapping using fast spin echo techniques - a linear correction procedure. Neuroimage 157, 476–485.
Oshio, K., Feinberg, D.A., 1991. GRASE (Gradient-and Spin-Echo) imaging: a novel fast MRI technique. Magn. Reson. Med. 20, 344–349.
Penny, W.D., Friston, K.J., Ashburner, J.T., Kiebel, S.J., Nichols, T.E., 2011. Statistical Parametric Mapping: the Analysis of Functional Brain Images. Elsevier Science.
Pike, G.B., 2012. Quantitative functional MRI: Concepts, issues and future challenges. Neuroimage 62, 1234–1240.
Poon, C.S., Henkelman, R.M., 1992. Practical T2 quantitation for clinical applications. J. Magn. Reson. Imag. 2, 541–553.
Powers, W.J., Clarke, W.R., Grubb Jr., R.L., Videen, T.O., Adams Jr., H.P., Derdeyn, C.P., Investigators, C., 2011. Extracranial-intracranial bypass surgery for stroke prevention in hemodynamic cerebral ischemia: the Carotid Occlusion Surgery Study randomized trial. J. Am. Med. Assoc. 306, 1983–1992.
Prasloski, T., Madler, B., Xiang, Q.S., MacKay, A., Jones, C., 2012a. Applications of stimulated echo correction to multicomponent T2 analysis. Magn. Reson. Med. 67, 1803–1814.
Prasloski, T., Rauscher, A., MacKay, A.L., Hodgson, M., Vavasour, I.M., Laule, C., Madler, B., 2012b. Rapid whole cerebrum myelin water imaging using a 3D GRASE sequence. Neuroimage 63, 533–539.
Preibisch, C., Shi, K., Kluge, A., Lukas, M., Wiestler, B., Gottler, J., Gempt, J., Ringel, F., Al Jaberi, M., Schlegel, J., Meyer, B., Zimmer, C., Pyka, T., Forster, S., 2017. Characterizing hypoxia in human glioma: a simultaneous multimodal MRI and PET study. NMR Biomed. 30.
Sedlacik, J., Boelmans, K., Löbel, U., Holst, B., Siemonsen, S., Fiehler, J., 2014. Reversible, irreversible and effective transverse relaxation rates in normal aging brain at 3T. Neuroimage 84, 1032–1041.
Seiler, A., Lauer, A., Deichmann, R., Noth, U., You, S.J., Pfeilschifter, W., Singer, O.C., Pilatus, U., Wagner, M., 2019. Complete restitution of the ischemic penumbra after successful Thrombectomy : a pilot study using quantitative MRI. Clin. Neuroradiol. 29 (3), 415–423.
Shu, C.Y., Herman, P., Coman, D., Sanganahalli, B.G., Wang, H., Juchem, C., Rothman, D.L., de Graaf, R.A., Hyder, F., 2016a. Brain region and activity-dependent properties of M for calibrated fMRI. Neuroimage 125, 848–856.
Shu, C.Y., Sanganahalli, B.G., Coman, D., Herman, P., Rothman, D.L., Hyder, F., 2016b. Quantitative beta mapping for calibrated fMRI. Neuroimage 126, 219–228.
Smith, A.J., Blumenfeld, H., Behar, K.L., Rothman, D.L., Shulman, R.G., Hyder, F., 2002. Cerebral energetics and spiking frequency: the neurophysiological basis of fMRI. Proc. Natl. Acad. Sci. U. S. A. 99, 10765–10770.
Stone, A.J., Blockley, N.P., 2017. A streamlined acquisition for mapping baseline brain oxygenation using quantitative BOLD. Neuroimage 147, 79–88.
Stone, A.J., Holland, N.C., Berman, A.J.L., Blockley, N.P., 2019. Simulations of the effect of diffusion on asymmetric spin echo based quantitative BOLD: an investigation of the origin of deoxygenated blood volume overestimation. Neuroimage 201, 116035.
Toth, V., Forschler, A., Hirsch, N.M., den Hollander, J., Kooijman, H., Gempt, J., Ringel, F., Schlegel, J., Zimmer, C., Preibisch, C., 2013. MR-based hypoxia measures in human glioma. J. Neuro Oncol. 115, 197–207.
Uddin, M.N., Marc Lebel, R., Wilman, A.H., 2013. Transverse relaxometry with reduced echo train lengths via stimulated echo compensation. Magn. Reson. Med. 70, 1340–1346.
Ulrich, X., Yablonskiy, D.A., 2015. Separation of cellular and BOLD contributions to T2* signal relaxation. Magn. Reson. Med. 75, 606–615.
Wagner, M., Helfrich, M., Volz, S., Magerkurth, J., Blasel, S., Porto, L., Singer, O.C., Deichmann, R., Jurcoane, A., Hattingen, E., 2015. Quantitative T2, T2*, and T2' MR imaging in patients with ischemic leukoaraiosis might detect microstructural changes and cortical hypoxia. Neuroradiology 57, 1023–1030.
Wagner, M., Magerkurth, J., Volz, S., Jurcoane, A., Singer, O.C., Neumann-Haefelin, T., Zanella, F.E., Deichmann, R., Hattingen, E., 2012. T2'- and PASL-based perfusion mapping at 3 Tesla: influence of oxygen-ventilation on cerebral autoregulation. J. Magn. Reson. Imag. 36, 1347–1352.
Whittall, K.P., MacKay, A.L., Graeb, D.A., Nugent, R.A., Li, D.K., Paty, D.W., 1997. In vivo measurement of T2 distributions and water contents in normal human brain. Magn. Reson. Med. 37, 34–43.
Whittall, K.P., MacKay, A.L., Li, D.K., 1999. Are mono-exponential fits to a few echoes sufficient to determine T2 relaxation for in vivo human brain? Magn. Reson. Med. 41, 1255–1257.
Wiestler, B., Kluge, A., Lukas, M., Gempt, J., Ringel, F., Schlegel, J., Meyer, B., Zimmer, C., Förster, S., Pyka, T., Preibisch, C., 2016. Multiparametric MRI-based differentiation of WHO grade II/III glioma and WHO grade IV glioblastoma. Sci. Rep. 6, 35142.
Yablonskiy, D.A., Haacke, E.M., 1994. Theory of NMR signal behavior in magnetically inhomogeneous tissues: the static dephasing regime. Magn. Reson. Med. 32, 749–763.